Modeling of Iron Losses of Permanent-Magnet Synchronous Motors

Chunting Mi, *Member, IEEE*, Gordon R. Slemon, *Life Fellow, IEEE*, and Richard Bonert, *Member, IEEE*

***Abstract*—Permanent-magnet (PM) motors offer potential energy savings as compared with induction motors because of the virtual elimination of rotor loss and the reduction of stator loss from operation near unity power factor. In PM machines, iron losses form a significant fraction of the total loss partly due to the nonsinusoidal flux density distribution. Design optimization therefore requires good means of predicting these iron losses. Finite-element analysis can be employed but this approach is cumbersome and costly when used in the many iterations needed in optimizing the design. This paper presents a set of improved approximate models for the prediction of iron loss. They can be used in design optimization programs and, since they are directly related to machine dimensions and material properties, they also provide quick insight into the effects of design changes. A time-stepped finite-element method is employed to evaluate the iron losses in a range of typical PM machines and the results are used to evaluate the adequacy of the models. The predictions of overall iron losses are then compared with measurements made on two PM motors.**

***Index Terms*—Core losses, eddy currents, hysteresis, iron losses, permanent magnets (PMs), permanent-magnet (PM) machines, synchronous motors.**

I. Introduction

PERMANENT-MAGNET (PM) motors are challenging the monopoly of induction machines in many applications such as pumps, fans, and compressor drives where the higher initial cost can be rapidly paid back by energy savings [1]. In PM motors, iron losses form a larger proportion of the total losses than is usual in induction machines. This is partly due to the elimination of significant rotor slip loss and is partly due to the reduction of stator loss from operation at near-unity power factor. Optimum design of PM motors therefore requires good means for predicting these iron losses [2]. It is accepted that finite-element analysis can produce a good estimate of iron losses but this approach is cumbersome and costly when used in the many iterations needed in the optimizing design. This paper presents a set of improved approximate models for the prediction of iron losses of surfaced-mounted PM motors.

An earlier paper [3] developed expressions for iron losses of surface-mounted PM motors based on a number of approximations. This simple analytical iron-loss model has been used by a few authors to determine the iron losses of PM synchronous motors [4]–[8]. While the overall application of these approximations produced an acceptable prediction of the total measured losses in an experimental machine, the validity of each approximation remained in doubt. In this paper, these approximations are examined in turn and their results are compared with those obtained by finite-element analysis.

Paper IPCSD 03–009, presented at the 2001 Industry Applications Society Annual Meeting, Chicago, IL, September 30–October 5, and approved for publication in the IEEE TRANSACTIONS ON INDUSTRY APPLICATIONS by the Electric Machines Committee of the IEEE Industry Applications Society. Manuscript submitted for review June 19, 2002 and released for publication January 23, 2003.

C. Mi is with the Department of Electrical and Computer Engineering, University of Michigan, Dearborn, MI 48128-1491 USA (e-mail: mi@ieee.org).

G. R. Slemon and R. Bonert are with the Department of Electrical and Computer Engineering, University of Toronto, Toronto, ON M5S 3G4, Canada (e-mail: g.slemon@utoronto.ca; r.bonert@utoronto.ca).

Digital Object Identifier 10.1109/TIA.2003.810635

II. Iron Loss Density

Measurements of iron losses in magnetic material are traditionally made with sinusoidal flux density of varying frequency and magnitude. The total iron-loss density p_{iron} is commonly expressed in the following form for sinusoidally varying magnetic flux density B with angular frequency ω_s:

$$p_{\text{iron}} = p_h + p_e = k_h B^{\beta} \omega_s + k_e B^2 \omega_s^2 \text{ W/m}^3 \tag{1}$$

where p_h and p_e are the hysteresis and the eddy-current loss density, respectively, k_h and k_e are hysteresis and eddy current constants, and β is the Steinmetz constant, all of which depend on the lamination material. These constants can be obtained by curve fitting from manufacturer's data. Typical values for grades of silicon iron laminations used in small and medium induction motors, with the stator frequency given in radians per second, are in the ranges $k_h = 40$–55, $\beta = 1.8$–2.2, and $k_e = 0.04$–0.07.

An expression for the classical eddy-current loss can also be developed based on the resistivity of the core material [14]. The result is generally found less than that obtained from the second term of (1).

The iron-loss expression in (1) is only valid for sinusoidal flux density. In most PM motors, the variation in flux density in the stator core is far from sinusoidal. In this situation, while the hysteresis loss is still easy to evaluate as it depends only on the peak value of the flux density assuming that there are no minor hysteresis loops, the eddy-current losses evaluated using only the fundamental component of flux density may be much lower than the measured values [9]. An alternative approach which includes the harmonics of the flux density can be employed [10]–[13], but this approach involves the complex evaluation of these harmonics in each finite element of the machine.

For the eddy current it is convenient to represent the average loss density as a function of the time rate of change of the vector flux density [3], [14]

$$p_e = \frac{2k_e}{T} \int_0^T \left(\frac{d\mathbf{B}}{dt} \right)^2 dt \text{ W/m}^3 \tag{2}$$

where T is the period. For a p-pole machine rotating at ω_{mech} rad/s, the time period for one cycle is

$$T = \frac{1}{f} = \frac{4\pi}{p\omega_{\mathrm{mech}}} \quad \text{(s)}. \tag{3}$$

Use of (2) assumes that the eddy-current losses are induced by the field variation, whether it is pulsating or rotating [15]. The eddy-current loss is related not only to the magnitude of the flux density, but also to the way in which each of the two orthogonal components of the flux density changes [14], [16].

In this paper, (2) is employed to calculate eddy-current losses. The rotational flux will be decomposed to two orthogonal components: radial (normal) and circumferential (longitudinal) components to evaluate the iron losses.

III. Time-Stepped Finite-Element Analysis

Although it requires high effort for general use in most designs and is not practical during the preliminary PM motor design iteration stages, time-stepped finite-element method (FEM) remains the most powerful and precise tool to calculate electromagnetic field distributions and field-related parameters [8]–[12]. Time-stepped FEM is also used as an effective tool to verify loss calculation based on simpler loss models [4], [5], [17], [18], as it is economically and technically impractical to verify all loss predictions with experiments.

A time-stepped FEM was employed to calculate iron loss numerically in this paper. The results of these analyses are then used to validate and refine the assumptions involved in approximate loss models. The PM motor contains a standstill stator and a moving rotor. In establishing the meshes for the analysis, the rotor is moved and positioned at each time step such that it does not disturb the integrity of the mesh structure as it moves. The initial meshes of the stator and the rotor are generated such that half of the air gap belongs to the stator and the other half to the rotor. A stator mesh and a rotor mesh share the same boundary at the middle of the air gap. The inner stator circumference at the air gap and the outer rotor circumference are divided into equal steps so that their nodes coincide. To provide for movement of the rotor, the time step is chosen so that the angle or length of each step is equal to the interval between two neighboring nodes along the mid air gap. Because of periodicity of the magnetic field, only one pair of poles needs to be modeled. Similarly, because of the half-wave symmetry of flux density, only half of the time period T needs to be calculated.

The radial (x) and circumferential (y) components of flux density at time step t_n in the volume element m are evaluated as $B_{mx,n}$ and $B_{my,n}$. The total eddy-current loss can be obtained from (2) as

$$\begin{aligned} P_e =& \frac{p}{2}\sum_{m=1}^{M} A_m l_{fe}\frac{2k_e}{T}2\int_0^{T/2}\left(\frac{d\mathbf{B}}{dt}\right)^2 dt \\ =& 2pNk_e l_{fe} f^2 \\ & \times \sum_{m=1}^{M}\left\{ A_m\left[\sum_{n=1}^{N}(B_{mx,n}-B_{mx,n-1})^2 \right.\right. \\ & \left.\left. +\sum_{n=1}^{N}(B_{my,n}-B_{my,n-1})^2\right]\right\} \text{ W} \end{aligned} \tag{4}$$

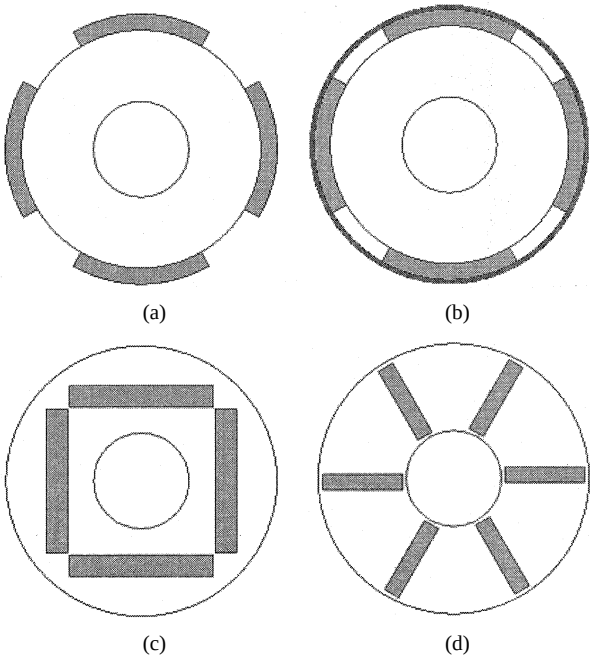

Fig. 1. Major rotor configurations of PM machines. (a) Rotor with surface-mounted magnets. (b) Rotor with surface-mounted magnets and sleeve ring. (c) Rotor with inset magnets. (d) Rotor with circumferential magnets.

where N is the total number of steps in the half time period $T/2$, l_{fe} is the stator core length, A_m is the area of element m, and M is the total number of elements in the teeth and the yoke of the stator.

Similarly, the total hysteresis loss can be expressed as

$$P_h = 2\pi f k_h l_{fe}\sum_{m=1}^{M}\left[A_m B_{m,\max}^{\beta}\right] \text{ W} \tag{5}$$

where $B_{m,\max}$ is the maximum flux density of element m.

IV. Review of Previous Analytical Iron-Loss Model

In the preliminary study on iron losses of surface-mounted PM motors [3], a number of tentative conclusions were derived based on a series of assumptions.

The assumptions and conclusions of [3] can be summarized as follows.

1) The eddy-current loss was assumed to be dependent on the square of time rate of change of the flux density vector in the stator core.
2) The tooth eddy-current loss was assumed to be concentrated in those teeth which are near the edges of the surface-mounted magnets and, thus, was independent of the angular width of magnets.
3) The flux density in a tooth was assumed to be approximately uniform.
4) As the magnet rotates, the flux density in a stator tooth at the leading edge of the magnet was assumed to rise linearly from zero to a maximum and then remain essentially constant while the magnet passes. At the lagging edge, the tooth flux drops from maximum to zero in the same pattern.

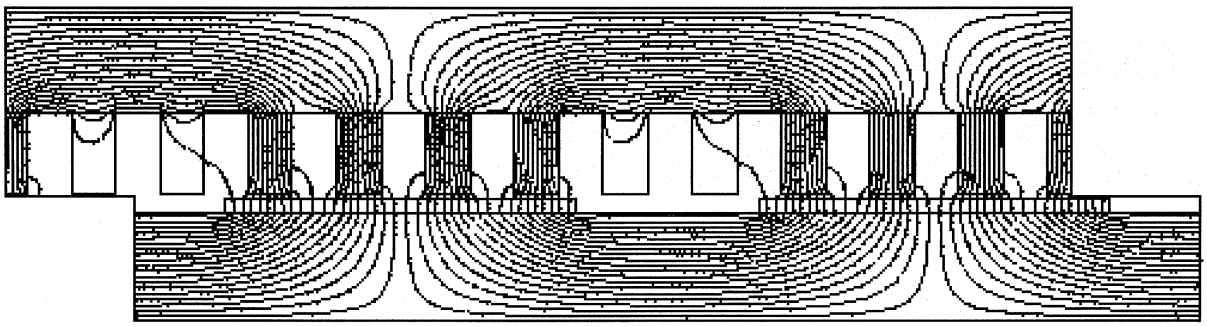

Fig. 2. Configuration and flux distribution of a linear PM synchronous motor in a pair of poles. The linear machine has two slots per pole phase and is surface mounted with rectangular-edged parallel-magnetized magnets. Assuming it has a large number of poles. Main dimensions of the machine are as follows: air-gap length $\delta = 1$ mm; pole pitch $\tau = 100.8$ mm; both tooth and slot width $w_o = w_s = 8.4$ mm; magnet thickness $l_m = 3.5$ mm; slot pitch $\lambda = 16.8$ mm.

5) The rise or fall time of the tooth flux density was assumed to be the time interval for the magnet edge to traverse one tooth width.
6) For a given torque and speed rating, the tooth eddy current loss was stated as approximately proportional to the number of poles divided by the width of a tooth. Alternatively, the tooth eddy current loss was approximately proportional to the product of poles squared and slots per pole-phase.
7) For a given frequency, the tooth eddy-current loss was stated to be proportional to the number of slots per pole phase.
8) The eddy-current loss in the stator yoke was approximated using only the circumferential component of yoke flux density.

While the overall application of these approximations produced an acceptable prediction of the total measured losses in an experimental machine, the validity of each individual approximation remained in doubt. The uncertainties in these models are as follows:

1) the validity and accuracy of the derived flux waveform, both in the teeth and in the yoke;
2) the error caused by only using the magnitude of the flux density;
3) the error caused by neglecting geometry effects on flux waveforms and eddy-current loss of the motors.

In this paper, these assumptions are examined in turn and their results are compared with those obtained by time-stepped FEM.

V. Simplified Tooth Eddy-Current-Loss Model

Among the major types of rotor structures, rotors with surface-mounted magnets as shown in Fig. 1(a) are commonly used in PM synchronous motors for their simplicity. The drawback of the configuration is that the magnets may easily fly away from the surface at high speeds if they are originally glued on the rotor surface. The author has experienced several times the magnets flying off the rotor surfaces during the operation of PM motors. One effective way to avoid the mechanical weakness of surface-mounted PM synchronous motors is to bond the magnets with a cylindrical sleeve made of high-strength alloy as shown in Fig. 1(b) [19]–[21]. Rotors with interior magnets as shown in Fig. 1(c) and (d) can provide a more secure magnet setting.

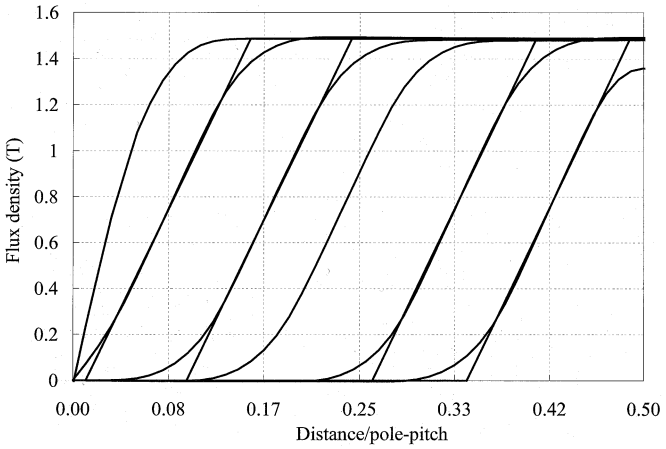

Fig. 3. Calculated tooth flux waveforms of the linear PM motor of Fig. 2 with variable magnet width. From left to right, I: $\alpha = 0.990$; II: $\alpha = 0.833$; III: $\alpha = 0.667$; IV: $\alpha = 0.532$; V: $\alpha = 0.333$; VI: $\alpha = 0.167$.

It can also produce more maximum torque due to its unequal d-axis and q-axis reluctance [22].

Although the simplified iron-loss model has been developed in the paper based on surfaced-mounted PM motors, it can also be adapted to predicting iron losses in interior-type and circumferential-type PM motors.

A. Tooth Flux Waveforms

Fig. 2 shows a typical flux density distribution in a surface-mounted PM motor with teeth of uniform width and with no stator current. In developing the loss models of the earlier paper [3], it was assumed that the flux density in each tooth was uniform and radially directed. It was time invariant for those teeth which were fully over the magnet, and that it varied linearly as the magnet edge passed under each end tooth. To test the assumption that eddy loss occurs only in the end teeth, an FEM was performed on one pair of poles of the linearly arranged machine as shown in Fig. 2.

The analysis was performed such that as the width of the magnet was changed, the number and shape of slots and teeth were kept constant. The normal component of flux density obtained at the center of a tooth is shown in Fig. 3. It can be seen that the rise of the flux follows almost a linear pattern except at the beginning and end of the change. The time for the approximated linear flux density to change from zero to plateau

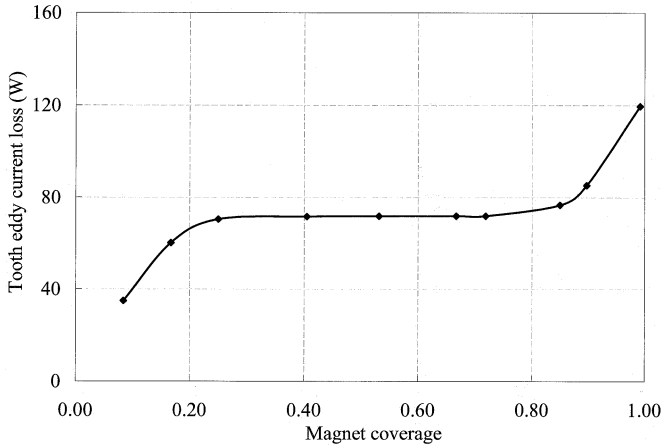

Fig. 4. Tooth eddy-current loss versus magnet coverage predicted by FEM.

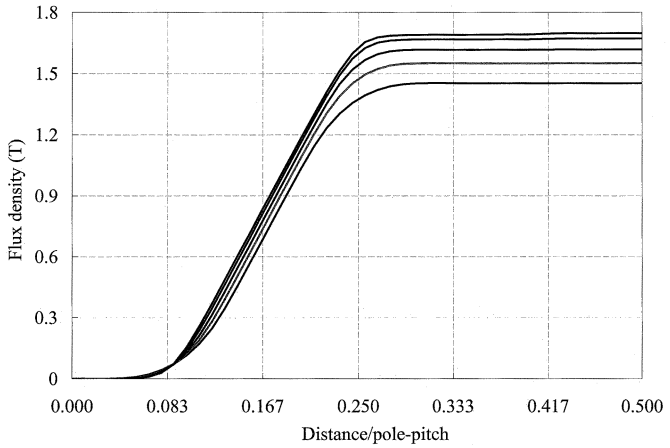

Fig. 5. Tooth flux density waveforms by changing the slot closure b_o. From top to bottom, slot closures are 1.6, 3.2, 5.0, 6.6, and 8.4 mm.

was found to be equivalent to that required for the magnet edge to traverse one slot pitch. This is in contrast to the assumption made in [3] that the linear change would occur as the magnet edge travels one tooth width.

It can also be seen from Fig. 3 that changing magnet width over a wide range does not change the achieved maximum flux density in the teeth, nor does it change the slope of the tooth flux waveforms. However, when the space between the two adjacent magnets is less than one slot pitch, the slope of tooth flux density begins to increase. Especially when magnet coverage approaches 1.0, the slope of the tooth flux density is dramatically increased. At the other extreme, when the magnet width is less than one slot pitch, the tooth flux density does not reach a plateau although the slope of the flux density waveform is still the same.

The calculated tooth eddy losses are shown in Fig. 4. It can be seen that the loss remains substantially constant as the magnet width is varied over a wide range. When the magnet width is less than about one slot pitch, no tooth has constant flux density. On the other extreme, when the space between two magnets is less than about one slot pitch, the eddy-current loss is considerably increased due to the increase of the circumferential flux in the teeth between magnets.

Next, the effect of slot closure was studied. An FEM analysis was performed on the linear PM machine to determine the average flux density at the center of a tooth over a time period $T/4$. The calculated tooth flux waveforms are shown in Fig. 5 as a function of slot closure.

It can be seen in Fig. 5 that the flux density varies approximately linearly. As expected, the plateau of tooth flux density increases as the slot opening is reduced. The time interval needed for the approximately linear flux change from zero to maximum is seen to be essentially constant and independent of the amount of slot closure.

B. Eddy Loss Induced by the Normal Component

A revised approximate model for tooth eddy-current loss can now be developed. For an m-phase PM motor with q slots per pole phase, there are mq slots per pole. The time Δt required for the magnet to traverse one slot pitch is

$$\Delta t = \frac{T}{2}\frac{1}{mq}. \tag{6}$$

Under linear trapezoidal assumptions of the waveforms, the time rate of tooth flux change is

$$\frac{dB}{dt} = \frac{B_{th}}{\Delta t}. \tag{7}$$

The change of tooth flux density occurs four times per time period T. The average eddy-current loss density in the teeth can now be expressed as

$$\begin{aligned} p_{et} =& 2k_e\left(\frac{B_{th}}{\Delta t}\right)^2\left(\frac{4\Delta t}{T}\right) = 16k_e mq\left(B_{th}f\right)^2 \\ =& \frac{12}{\pi^2}qk_e\left(\omega_s B_{th}\right)^2 \text{ W/m}^3. \end{aligned} \tag{8}$$

It can be seen that the eddy-current loss is proportional to the number of slots per pole phase q.

C. Effect of Motor Geometry

The effect of motor geometry was then studied [23]. For each geometrical change of the linear machine, the tooth eddy loss was calculated by FEM and compared to that predicted by approximation model (8). The ratio of these two predicted losses was introduced as a correction factor to the approximation model. It was found that the correction factor is a function of slot pitch, magnet thickness and air-gap length as shown in Fig. 6.

D. Eddy Loss Induced by the Longitudinal Component

So far, only the normal component of tooth flux density has been considered. FEM shows that although the magnitude of the longitudinal component of tooth flux density is negligible at the center of a tooth, it is comparable to the normal component at the shoes and surfaces of the tooth. In order to quantify this loss component, the eddy loss induced by the longitudinal component is calculated by FEM and compared to that predicted by the approximation model for different geometries. A second correction factor was then introduced to reflect the contribution of the

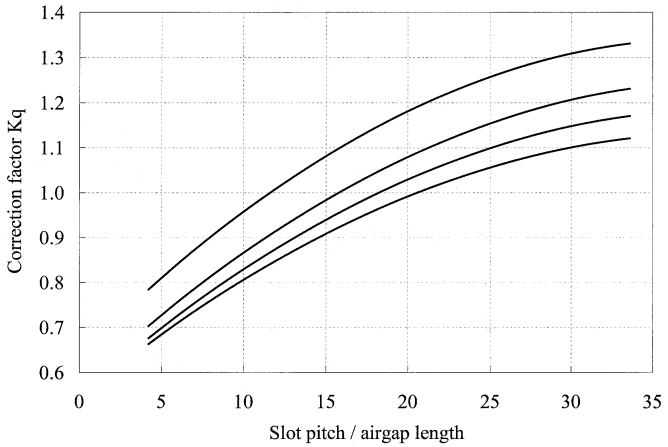

Fig. 6. Correction factor k_q as a function of motor geometry. From top to bottom: $l_m/\delta = 1.5,\ 3.0,\ 4.5$ and 6.0.

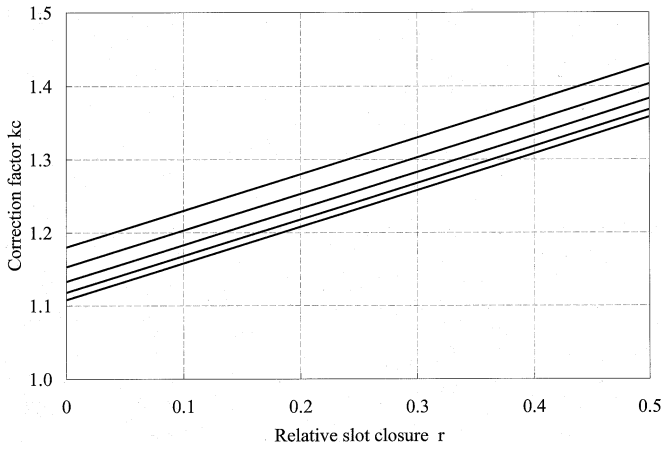

Fig. 7. Correction factor k_c with regard to slot closure γ, air gap, and tooth width, where γ is the ratio of slot closure to slot pitch: $\gamma = (w_s - w_o)/\lambda$, w_s is slot width, and w_o is slot openings. $\gamma = 0$ for open slot and $\gamma = 0.5$ for closed slot. From top to bottom: $\lambda/\delta = 32.6$; $\lambda/\delta = 16.8$; $\lambda/\delta = 11.2$; $\lambda/\delta = 8.4$; and $\lambda/\delta = 6.7$.

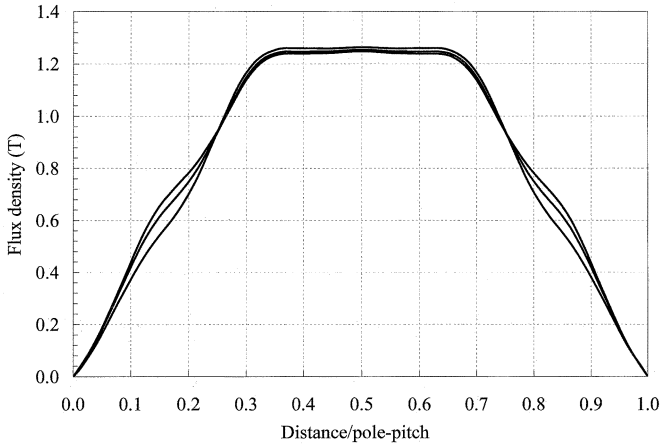

Fig. 8. Longitudinal component of flux at different layers of the stator yoke computed by FEM. From top to bottom: 1/3 yoke thickness from the tooth; at the middle of yoke; and 1/3 yoke thickness from the stator surface.

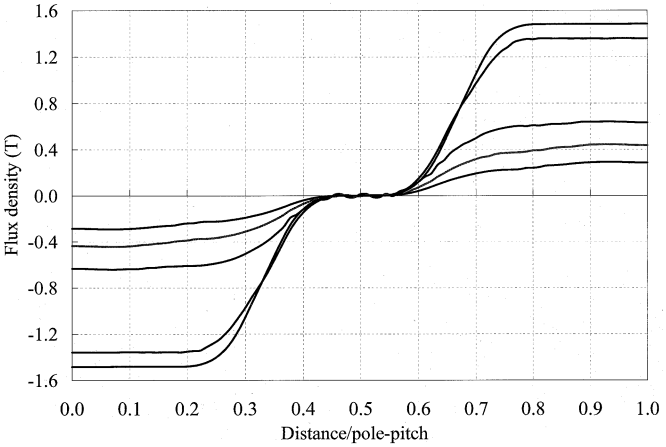

Fig. 9. Normal component of flux at different layers of the stator yoke computed by FEM. From top to bottom (above x axis): I—center of a tooth; II—1 mm from the tooth; III—1/3 yoke thickness from the tooth; IV—middle of yoke; and V—1/3 yoke thickness from the stator surface.

eddy loss induced by the longitudinal component as shown in Fig. 7.

E. Modified Tooth Eddy-Current-Loss Model

The modified tooth eddy-current-loss model can now be expressed as

$$p_{et} = \frac{4m}{\pi^2} q k_q k_c k_e (\omega_s B_{th})^2 \ \text{W/m}^3 \tag{9}$$

where k_q and k_c are correction factors which can be found from Figs. 6 and 7, respectively.

VI. Yoke Eddy-Current-Loss Model

A. Yoke Flux Waveforms

The flux pattern of Fig. 2 suggests that the circumferential component of the flux density in the yoke is roughly constant over the thickness of the yoke. It increases approximately linearly from the middle point of the magnet to the edge of the magnet and that it remains approximately constant in the yoke sector not above the magnet. The approximate model of the previous paper [3] was based on these assumptions. The radial component of yoke flux density was ignored.

Fig. 8 shows the longitudinal component of the yoke flux density at different layers of the yoke computed by FEM. It can be seen that the longitudinal component is approximately trapezoidal. The flux is approximately evenly distributed over the thickness of the yoke and the rise time of flux from negative plateau to positive plateau is approximately the time needed for one point in the yoke to traverse the magnet width.

Fig. 9 shows the normal component of yoke flux density computed by FEM at different layers of the yoke. It can be seen that the normal component has a similar waveform to that of tooth flux density waveform. The plateau of the flux at each layer of the yoke is different. The plateau is at its maximum near the tooth and drops dramatically penetrating further into the yoke and approaches zero near the surface of the yoke.

B. Eddy Loss Induced by the Longitudinal Component

Based on the above observation, a simplified yoke eddy-current-loss model can be developed.

The magnet coverage can be expressed as a function of magnet width as follows:

$$\alpha = \frac{w_m}{\frac{2\pi r}{p}} \tag{10}$$

where w_m is the width of the magnet which can be expressed alternatively as the fraction of the stator periphery covered by magnets.

The time interval required for one magnet of width w_m to pass a point in the stator yoke is

$$\Delta t = \frac{p w_m}{2 r \omega_s} = \frac{\alpha \pi}{\omega_s}. \tag{11}$$

During this time interval, the longitudinal flux component changes from $-B_c$ to B_c. Thus, the change rate of flux density over the fraction of time Δt is

$$\frac{dB_c}{dt} = \frac{2B_c}{\Delta t} = \frac{2\omega_s B_c}{\alpha \pi}. \tag{12}$$

During the remainder of the time the longitudinal flux density is assumed constant. Using (2), the eddy-current-loss density in the yoke caused by the longitudinal flux density component is then given by

$$p_{eyc} = \frac{1}{\alpha}\frac{8}{\pi^2} k_e \omega_s^2 B_c^2 \text{ W/m}^3. \tag{13}$$

C. Eddy Loss Induced by the Normal Component

Since at each layer of the yoke the normal component of yoke flux density has a different plateau, it is desirable to integrate the loss over the whole yoke to get the total eddy loss induced by the normal component. It was found that this component of loss can be expressed as

$$p_{eyr} \approx \frac{64 k_q d_y^2}{27 q \pi^2 \alpha^2 \lambda_2^2} k_e \omega_s^2 \hat{B}_c^2 \text{ W/m}^3 \tag{14}$$

where d_y is yoke thickness, and λ_2 is the projected slot pitch at the middle of yoke.

D. Simplified Yoke Eddy-Current-Loss Model

The modified yoke eddy-current-loss model can now be expressed as

$$p_{ey} = \frac{1}{\alpha}\frac{8}{\pi^2} k_e k_r \omega_s^2 B_c^2 \text{ W/m}^3 \tag{15}$$

where k_r is a correction factor for the eddy loss induced by the normal component of yoke flux density and is related to motor geometry

$$k_r = 1 + \frac{8 k_q d_y^2}{27 \alpha q \lambda_2^2}. \tag{16}$$

VII. Comparison of Iron Losses Predicted by Approximate Model and FEM

A. Tooth and Yoke Hysteresis Loss

Tooth hysteresis loss and yoke hysteresis loss can be expressed simply as a function of the maximum flux density in each area. In the teeth, the hysteresis loss density is

$$p_{ht} = k_h \omega_s B_{th}^{\beta} \text{ W/m}^3. \tag{17}$$

In the yoke, the hysteresis loss density is

$$p_{hy} = k_h \omega_s B_{yk}^{\beta} \text{ W/m}^3. \tag{18}$$

B. Total Iron Losses

Total iron losses are obtained by summing the eddy-current losses and hysteresis losses in the teeth and yoke

$$p = (p_{et} + p_{ht}) V_t + (p_{ey} + p_{hy}) V_y \text{ W} \tag{19}$$

where V_t and V_y are the volume of stator teeth and stator yoke.

C. Comparison of Predicted Iron Losses

The approximation model was applied to a number of PM motors to predict the iron losses [23]. Good agreements have been maintained between the iron losses predicted by the approximation model and those calculated by FEM. A three-phase 5-hp four-pole 1800-r/min surface-mounted PM motor is presented here for verification. A cross section of the motor along with its meshes and flux distribution is shown in Fig. 10. The dimensions and parameters are shown in Table I. Eddy-loss constant $k_e = 0.07$, and hysteresis constant $k_h = 44$.

Fig. 11 shows the tooth flux density waveform of the experimental PM motor obtained at the center of a tooth calculated by FEM. It can be measured from Fig. 11 that the distance needed for the linear part of the normal component of the tooth flux density to rise from zero to the plateau value is 0.128 pole pitch or 1.15 slot pitch. From the dimensions of the motor, it can be calculated that $l_m/\delta = 3.15$, and $\lambda/\delta = 5.1$. From Fig. 6, $k_q = 0.72$. From Fig. 7, $k_c = 1.18$. The tooth eddy loss of this motor is 17.3 W calculated by FEM at 1800 r/min. It is 18 W predicted by the approximation model (3.9% discrepancy).

Fig. 12 shows the yoke flux density waveforms of the experimental PM motor obtained at the middle of the stator yoke calculated by FEM. It can be seen from Fig. 12 that the linear part of the circumferential component of yoke flux density takes 0.3 pole pitch to rise from zero to the plateau. This confirms that the circumferential component takes about one magnet width to change from negative plateau to positive plateau. The normal component takes 0.13 pole pitch to rise from zero to plateau. Recall that the normal component of tooth flux density of this motor takes 0.128 pole pitch to rise from zero to plateau. It therefore confirms that the normal component of yoke flux density has the same waveform as that of the normal component of tooth flux density. By using the dimensions of the motor, $d_y = 17.4$ mm, $\lambda_2 = 15.1$ mm, and $k_q = 0.72$. From (16), $k_r = 1.14$. The yoke eddy loss of this motor is 18.1 W calcu-

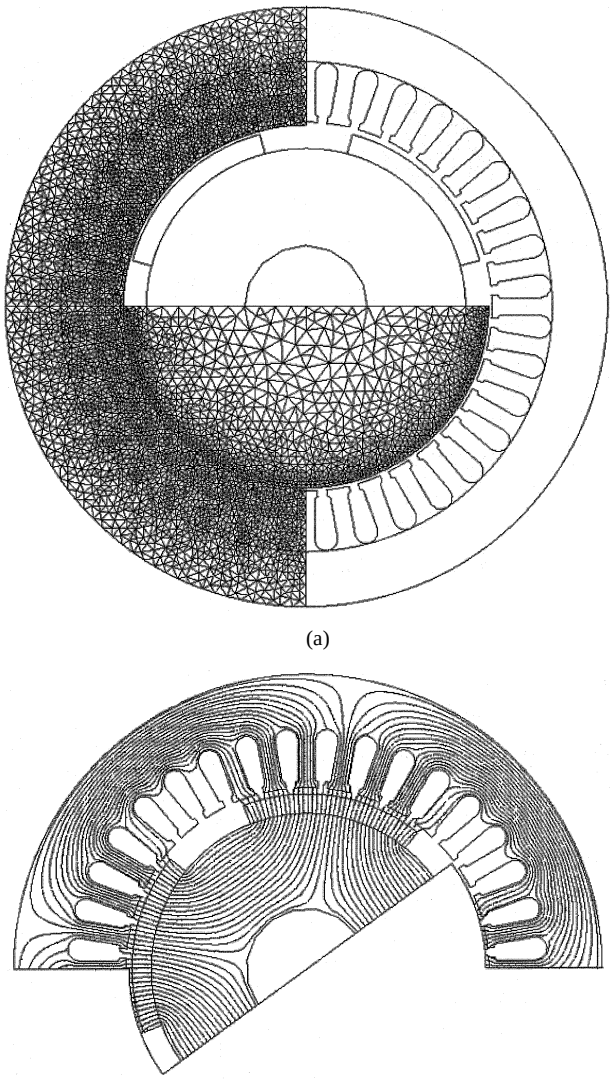

Fig. 10. A four-pole 36-slot rotary surface-mounted rectangular-edged radially magnetized PM motor. (a) Geometry and mesh. (b) Flux distribution.

TABLE I
DIMENSIONS AND PARAMETERS OF EXPERIMENTAL MOTOR

Name	Value	Name	Value
Inner radius of stator (mm)	58.5	Stator length (mm)	88.9
Outer radius of stator (mm))	95	Tooth width (mm)	5.3
Thickness of magnets (mm)	6.3	Yoke depth (mm)	17.4
Tooth flux density (T)	1.2398	Tooth height (mm)	19.1
Yoke flux density (T)	1.2827	Magnet coverage	0.667
Tooth volume ($m^{3)}$	0.000380	Slot opening (mm)	3
Yoke volume (m^3)	0.000838	Airgap length (mm)	2

lated by FEM at 1800 r/min. It is 19 W predicted by the approximation model (5% discrepancy).

Table II gives a comparison of the iron-loss components of the experimental PM motor obtained by FEM and by the approximate model for a number of values of speed. It shows good agreement between the predicted iron losses of the two methods.

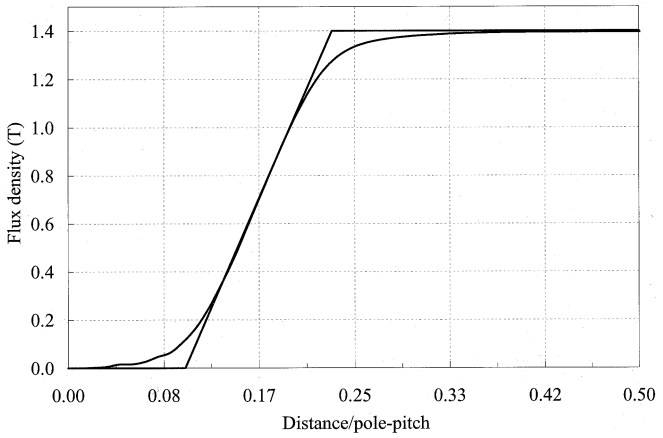

Fig. 11. Calculated radial component of flux density by FEM at the center of a tooth compared to a linearly approximated trapezoidal waveform.

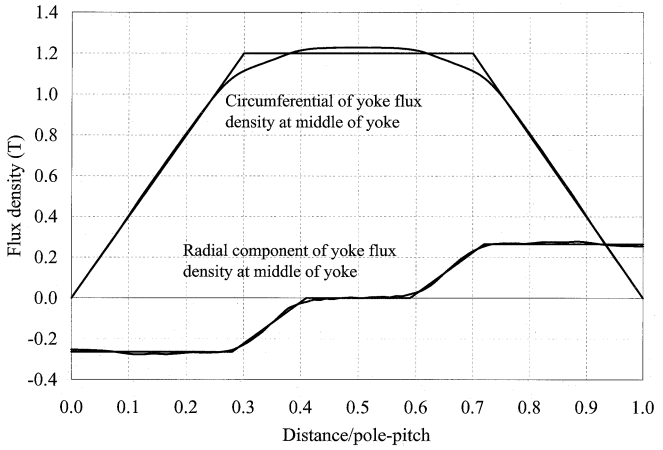

Fig. 12. Calculated yoke flux density by FEM at the middle of yoke compared to linearly approximated trapezoidal waveforms.

TABLE II
COMPARISON OF IRON LOSSES BETWEEN THAT CALCULATED BY FEM AND THAT PREDICTED BY THE APPROXIMATION MODEL (WATTS)

Speed (RPM)	300	600	900	1200	1500	1800
By simplified model	6.7	15.6	26.7	40.1	55.8	73.7
By FEM	6.5	15.0	25.5	37.9	52.3	68.7
Difference (%)	3.1	4.0	4.7	5.8	6.7	7.3

VIII. EXPERIMENTAL INVESTIGATION

The open-circuited PM motor was driven by a dynamometer and the shaft torque was measured over a wide range of speed. This torque–speed product represents the no-load loss of the motor. The loss consists of the iron loss plus the friction and windage loss. This latter component of losses cannot be measured directly on a PM motor since the field-produced iron loss is always present.

To circumvent this difficulty, the procedure in [14] was employed. An identical rotor without magnets on its surface was assembled with the same stator. When this motor is driven by the same dynamometer, the shaft torque represents the friction and windage loss of the motor. The friction and windage loss for the motor with and without PM on the rotor may be slightly different but the difference is ignored. This friction and windage

TABLE III
COMPARISON OF IRON LOSSES BETWEEN MEASURED AND PREDICTED (WATTS)

Speed (RPM)	300	600	900	1200	1500	1800
Predicted	6.7	15.6	26.7	40.1	55.8	73.7
Measured (with inverter)	4.2	11.9	22.8	36.3	52.6	71.6
Measured (by torque)	3.1	11.9	21.1	35.4	55.0	72.5

loss was subtracted from the total losses to obtain the iron losses at each value of operating speed.

A second measurement of losses was performed when the motor is driven with an inverter. With no mechanical load on the PM motor shaft, the input power at the stator terminals is measured. This power represents the total losses in the motor. Since the current is negligible at no load, the correction for copper loss is neglected. The iron losses are the total losses with the friction and windage loss of the machine subtracted.

Table III gives a comparison of the total iron losses of the experimental PM motor measured by these two methods and those predicted by the approximate model over a range of values of speed. The discrepancy between the predicted and the measured iron losses are generally within 5%.

IX. CONCLUSION

This paper has described an improved approximate model for predicting iron losses in surface-mounted PM synchronous machines.

Assumptions made in an earlier paper have been refined by comparison with FEM analysis. Experimental measurements have also been made to add confidence to the results.

These simple approximation models for iron losses should be of distinct value in design optimization studies where the large number of dimensional iterations precludes the use of finite-element analysis for loss prediction.

REFERENCES

[1] G. R. Slemon, "High-efficiency drives using permanent-magnet motors," in *Proc. Int. Conf. Industrial Electronics, Control and Instrumentation*, vol. 2, Maui, Hawaii, 1993, pp. 725–730.

[2] B. K. Bose, *Power Electronics and Variable Frequency Drives, Technology and Applications*. Piscataway, NJ: IEEE Press, 1997.

[3] G. R. Slemon and L. Xian, "Core losses in permanent magnet motors," *IEEE Trans. Magn.*, vol. 26, pp. 1653–1655, Sept. 1990.

[4] F. Deng, "An improved iron loss estimation for permanent magnet brushless machines," *IEEE Trans. Energy Conversion*, vol. 14, pp. 1391–1395, Dec. 1999.

[5] K. J. Tseng and S. B. Wee, "Analysis of flux distribution and core losses in interior permanent magnet motors," *IEEE Trans. Energy Conversion*, vol. 14, pp. 969–975, Dec. 1999.

[6] R. Rabinovici and T. J. E. Miller, "Eddy current losses of surface-mounted permanent magnet motors," *Proc. IEE—Elect. Power Applicat.*, vol. 144, no. 1, pp. 61–64, 1997.

[7] T. J. E. Miller and Rabinovici, "Back-emf waveforms and core losses of brushless DC motors," *Proc. IEE—Elect. Power Applicat.*, vol. 141, no. 3, pp. 144–154, 1994.

[8] R. Rabinovici, "Eddy current losses of permanent magnet motors," *Proc. IEE—Elect. Power Applicat.*, vol. 141, no. 1, pp. 7–11, 1994.

[9] G. Bertotti, A. A. Boglietti, M. Chiampi, D. Chiarabaglio, F. Fiorillo, and M. Lazzari, "An improved estimation of iron losses in rotation electrical machines," *IEEE Trans. Magn.*, vol. 27, pp. 5007–5009, Nov. 1991.

[10] J. G. Zhu, V. S. Ramsden, and P. A. Watterson, "Finite element calculation of core losses in motors with nonsinusoidal fields," in *Proc. ICEM'92*, Manchester, U.K., 1992, pp. 1182–1186.

[11] Z. J. Liu, K. J. Binns, and T. S. Low, "Analysis of eddy current and thermal problems in permanent magnet machines with radial field topologies," *IEEE Trans. Magn.*, vol. 31, pp. 1912–1915, July 1995.

[12] Z. J. Liu, C. Bi, and T. S. Low, "Analysis of iron loss in hard disk drive spindle motors," *IEEE Trans. Magn.*, vol. 33, pp. 4089–4091, Sept. 1997.

[13] M. K. Jamil and N. A. Demerdash, "Harmonics and core losses of permanent magnet DC motors controlled by chopper circuits," *IEEE Trans. Energy Conversion*, vol. 5, pp. 408–414, June 1990.

[14] G. R. Slemon, *Electrical Machines and Drives*. Reading, MA: Addison-Wesley, 1992.

[15] H. Yamada *et al.*, "Rotational core losses of induction motor by finite element method," *Elect. Eng. Jpn.*, vol. 103, no. 6, pp. 75–82, 1983.

[16] F. Fiorillo and A. Novikov, "An improved approach to power losses in magnetic laminations under nonsinusoidal induction waveform," *IEEE Trans. Magn.*, vol. 26, pp. 2904–2910, Sept. 1990.

[17] K. Atallah, Z. Q. Zhu, and D. Howe, "An improved method for predicting iron losses in brushless permanent magnet DC drives," *IEEE Trans. Magn.*, vol. 28, pp. 2997–2999, Apr. 1992.

[18] J. Gyselinck, L. Dupre, L. Vandevelde, and J. Melkebeek, "Calculation of iron losses in electrical machines using the Preisach model," in *Proc 3rd Int. Workshop Electrical and Magnetic Fields*, Liege, Belgium, 1996, pp. 423–428.

[19] V. B. Honsinger, "The fields and parameters of interior type AC permanent magnet machines," *IEEE Trans. Power App. Syst.*, vol. 101, pp. 867–876, Apr. 1992.

[20] K. J. Binns and M. S. N. Al-Din, "Use of canned rotors in high-fields permanent magnet machines," *Proc. Inst. Elect. Eng.*, vol. 139, no. 5, pp. 471–477, 1992.

[21] M. Chunting and J. Xiaoyin, "Effect of ring material on airgap flux of permanent magnet machines," *J. Northwestern Polytech. Univ.*, vol. 11, no. 4, pp. 447–450, 1993.

[22] G. R. Slemon, "Design of permanent magnet AC motors for variable speed drives," in *Performance and Design of Permanent Magnet AC Motor Drives*. New York: IEEE Press, 1991, ch. 3.

[23] C. Mi, "Modeling of iron losses of permanent magnet synchronous motors," Ph.D. dissertation, Dept. Elect. Comput. Eng., Univ. Toronto, Toronto, ON, Canada, 2001.

Chunting Mi (S'00–A'01–M'01) received the B.S.E.E. and M.S.E.E. degrees from Northwestern Polytechnical University, Xi'an, China, and the Ph.D degree from the University of Toronto, Toronto, ON, Canada, all in electrical engineering.

He is an Assistant Professor at the University of Michigan, Dearborn, with teaching responsibilities in the area of power electronics, electric vehicles, electric machines, and drives. From 2000 to 2001, he was an Electrical Engineer with General Electric Canada, Inc. He was responsible for designing and developing large electric motors and generators up to 30MW. He has taught power electronics and electric machines and drives courses for over ten years. He has offered the electric and hybrid vehicles course to graduate students at the University of Michigan and the U.S. Army TACOM. He has recently developed a Power Electronics and Electrical Drives Laboratory at the University of Michigan. His main interests are electric drives and power electronics circuits including induction, brushless dc, and PM synchronous; renewable energy systems; and electrical and hybrid vehicle powertrain design and modeling.

Dr. Mi is the Chair of the Power and Industrial Electronics Chapter of the IEEE Southeast Michigan Section.

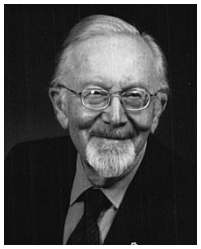

Gordon R. Slemon (S'46–A'48–M'48–SM'55–F'75–LF'90) received the B.A.Sc. and M.A.Sc. degrees from the University of Toronto, Toronto, ON, Canada, the D.I.C. of the Imperial College of Science and Technology, London, U.K., and the Ph.D. and D.Sc. degrees from the University of London, London, U.K.

Following employment with Ontario Hydro and Atomic Energy of Canada, he taught at Nova Scotia Technical College prior to his appointment to the staff of the Department of Electrical Engineering at the University of Toronto in 1955. He served as Head of its Electrical Engineering Department from 1966 to 1976, and as Dean of its Faculty of Applied Science and Engineering from 1979 to 1986. Currently, he acts as a Consultant to industry and government as well as continuing his research specialty of electric machines and drives. He is also Professor Emeritus in Electrical and Computer Engineering at the University of Toronto. He is the author or coauthor of five textbooks and 170 technical papers.

Dr. Slemon is an Officer of the Order of Canada and a Fellow of the Institution of Electrical Engineers, U.K., the Engineering Institute of Canada, and the Canadian Academy of Engineering. In 1990, he received the IEEE Nikola Tesla Award and IEEE Gold Medal.

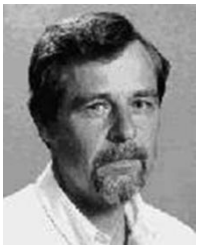

Richard Bonert (M'81) received the Dipl.-Ing. and Doctorate degrees in electrical engineering from the University of Karlsruhe, Karlsruhe, Germany, in 1969 and 1977, respectively.

He joined Brown Boveri, Germany, in 1969 as a Project Engineer, where he was engaged in designing electrical equipment for rolling mills, in particular, controlled electric drives. In 1971, he joined the Elektrotechnisches Institut, University of Karlsruhe, as a Research Associate and Chief Engineer for the experimental facilities. His area of research and teaching was power-semiconductor-controlled drives. After receiving a Research Fellowship, he worked in the Department of Electrical Engineering, University of Toronto, Toronto, ON, Canada, during 1978–1979. He joined the department in 1980 and is currently a Professor in the Power Systems and Devices Research Group. His main interests are power-semiconductor-controlled electric drives and power electronics circuits, and the application of programmable electronics circuits in this field. He has a strong interest in laboratories for power engineering to support graduate research and education in engineering.